Journal of Geochemical Exploration 155 (2015) 14–25

Contents lists available at ScienceDirect

Journal of Geochemical Exploration

journal homepage: www.elsevier.com/locate/jgeoexp

Using ion and isotope characterization to delimitate a hydrogeological macrosystem. Sierra de Gádor (SE, Spain)

A. Vallejos [a,*], M.A. Díaz-Puga [a], F. Sola [a], L. Daniele [b,c], A. Pulido-Bosch [a]

[a] Water Resources and Environmental Geology, University of Almería, Spain
[b] Department of Geology, FCFM, University of Chile, Chile
[c] Andean Geothermal Center of Excellence (CEGA), Fondap-Conicyt, Chile

ARTICLE INFO

Article history:
Received 13 March 2014
Accepted 20 March 2015
Available online 28 March 2015

Keywords:
Carbonate aquifer
Hydrogeochemistry
Local meteoric water line
Isotopes

ABSTRACT

Sierra de Gádor is a karstic macrosystem characterized by highly complex geometry. The two main economic activities in this area – the highly profitable irrigated agriculture and tourism – are supported by water resources from Sierra de Gádor, hence the interest in understanding this aquifer system. The highly variable precipitation in the area is characteristic of the arid conditions. The aim of the study presented in this paper was to define the principal hydrogeochemical and isotopic characteristics of the area and to characterize the different types of freshwater, some of which are affected by the process of mixing with saltwater – particularly those at the east and west extremes of the Sierra de Gádor. The hydrogeochemical analysis enabled the principal geochemical processes occurring in the aquifer to be established. The waters can be grouped into four categories, each defined by a distinctive solute. Dissolution of dolomite determines the chemical composition of less mineralized water. Dedolomitization (dolomite dissolution together with calcite precipitation caused by dissolution of gypsum) becomes predominant when the water flows through interbedded gypsum. Marine intrusion results in highly-mineralized waters and leads to base exchange reactions. The variation of $\delta^{18}O$ content with altitude (−0.19‰/100 m) allows the main recharge areas to be determined: 2000–1500 m a.s.l., 1500–900 m a.s.l., and below 900 m a.s.l., according to the different hydrodynamic characteristics of each area. In some sectors, it is possible to detect the current recharge from rainwater infiltration or seawater intrusion, based on its tritium content.

1. Introduction

A common characteristic of karstic aquifers is the complexity of their preferential flow pathways. Accordingly, it is necessary to look for tools that can help interpret these systems. Hydrogeochemical and isotope analyses can be used to test and fine-tune a conceptual hydrogeological model. Hydrochemistry and isotope composition of groundwater provides critical information about the sources of groundwater recharge, timing of recharge, water–rock interactions along the flow paths, and mixing of different groundwater bodies (Kanduč et al., 2012; Kohfahl et al., 2008; Pu et al., 2013; Wu et al., 2009).

The geochemical processes in carbonate aquifer systems have been well documented for many sites worldwide (e.g., Daniele et al., 2013; Hanshaw & Back, 1979; Hunkeler & Mudry, 2007; López-Chicano et al., 2001; Plummer et al., 1990; Wicks & Herman, 1996). The degree of hydrochemical evolution is largely determined by residence time of water within the aquifer, which determines the duration of the water–rock interaction (Moral et al., 2008). Sometimes, variations in hydrogeochemistry result from tectonic control of different catchment areas (Prtoljan et al., 2012). Dedolomitization, induced by gypsum dissolution, can be an important influence on the evolution of groundwater chemistry (Capaccioni et al., 2001; Cardenal et al., 1994; Ma et al., 2011; Plummer et al., 1990).

Environmentally stable, radiogenic isotopes – especially $\delta^{18}O$, $\delta^{2}H$, $\delta^{13}C$, $\delta^{34}S$ values and ^{14}C and ^{3}H activity – act as invaluable tracers of regional-scale hydrogeological processes (Clark & Fritz, 1997; Herczeg et al., 1997; Liotta et al., 2013; Mazor, 1991). Spatio-temporal isotope monitoring can allow the groundwater flowpaths and hydrodynamics in fissured and karstic aquifers to be defined, by taking into account the hydrogeological and hydrogeochemical settings (Barbieri et al., 2005). The stable isotope composition of rainfall ($\delta^{2}H$ and $\delta^{18}O$) is determined by climate and can be used as a groundwater tracer in hydrological studies (Clark & Fritz, 1997; Gat, 1996; Kendall & McDonnell, 1998; Lee & Krothe, 2001). Changes in isotopic composition along groundwater flow paths reflect the origin and history of the water (e.g., recharge and discharge processes, salinization and evaporation prior to recharge). Therefore, to determine the likely processes controlling groundwater recharge, it is essential to consider the amount and isotopic signature of individual rainfall events throughout the year (Gat, 1996; Gat & Airey, 2006; Ladouche et al., 2009).

Water in karstic aquifers can be classified by its $\delta^{13}C$. There are several sources of carbon dioxide contributing to the DIC in karstic

* Corresponding author.
E-mail address: avallejo@ual.es (A. Vallejos).

http://dx.doi.org/10.1016/j.gexplo.2015.03.006
0375-6742/

waters. Important sources include atmospheric CO_2, CO_2 from carbonate rock dissolution, biomineralization of soil organic matter and plant root respiration (Nhan et al., 2013).

The Sierra de Gádor mountain range in south-eastern Spain extends to 2250 m above sea level. The associated aquifer system is currently exploited to irrigate some 20,000 ha of highly profitable early-season greenhouse crops. Proliferation of greenhouses has led to a flourishing local economy, generating two billion dollars per year. In addition, the aquifer supplies more than 200,000 people with drinking water throughout the year, and more than double this number during the summer months. The area is characterized by a wide variability in annual precipitation, indicative of the arid conditions. The geometry of the system is highly complex.

This study employs geochemical and isotope approaches to devise an initial hydrogeological model for the Sierra de Gádor hydrogeological macrosystem, which encompasses groundwater recharge, circulation, chemical evolution and subsurface residence time. The specific objectives were: (1) to characterize the isotopic composition of the groundwater ($\delta^{18}O$, $\delta^{2}H$, $\delta^{13}C$, ^{3}H); (2) to determine sources and mechanisms of recharge; (3) to determine the dominant geochemical processes that influence groundwater chemistry; and, (4) to schematize groundwater flow patterns in this important hydrogeological region.

2. Hydrogeological setting

The study was carried out on Sierra de Gádor, situated in the province of Almería in the extreme southeast of Spain (Fig. 1). The surface area of this coastal mountain chain is close to 1000 km^2. The climate is Mediterranean characterized by warm, dry summers and mild winters. The amount of water available depends on the rainfall regime – and it rains seldom and irregularly. The semiarid character of the area arises due to the combination of a lack of precipitation (400 mm on the southern slopes of Sierra de Gádor), strong insolation (around 2900 h $year^{-1}$), interannual variability in precipitation (22–35%) and high potential evaporation (about 900 mm $year^{-1}$). Temperature increases from a mean of 16 °C on the top of the mountains to 18.7 °C on the foot, where January is the coldest month (10 °C) and August is the hottest (27.2 °C) (Martín-Rosales et al., 2007). The inflows that contribute to the aquifers are basically infiltration of rainfall over the unit, as well as runoff from the face of the Sierra de Gádor. Current outflows are almost exclusively a result of pumped abstractions.

Geologically, it belongs to the Internal Zones of the Betic Cordillera (Alpujarride Complex). The structure of the Alpujarride Complex is characterized by the superposition of a number of tectonic units or nappes. The entire superimposed nappe structure has been subject to important tensional and strike-slip events (Sanz de Galdeano et al., 1985), which have led to the development of basins, now filled with Neogene and Quaternary detritic material.

Two tectonic units have been identified in the area: Gádor and Felix. The Gádor unit consists of a basal layer of phyllite with quartzite intercalations, which has been assigned to the Permian–Triassic. The transition from this underlying formation to the limestone–dolomite layer above is usually a layer of calcoschist and marly limestone (Martin-Rojas et al., 2009). The upper part of the series is dolomitic, with limestone predominating towards the top. The whole series is approximately 1000 m thick. The formations of the Felix unit, like those of the Gádor one, consist of a basal metapellitic layer with a carbonate layer above. The carbonate layer is much thinner than its Gádor counterpart, normally less than 100 m. It is also Middle–Upper Triassic in age. The Gádor unit covers almost all the whole of Sierra de Gádor, exposing small klippen of the overlying Felix unit.

Above these materials are the Miocene deposits, made up of calcarenite in the outcropping sectors, and marl and gypsum beneath a Plioquaternary infill (Rodríguez-Fernández & Martín-Penela, 1993). Quaternary deposits are present along the whole of the base of the southern face of the Sierra, making up large alluvial fans that occasionally exceed 150 m in thickness. In the western sector, the Berja intramountain basin is filled with Neogene and Quaternary deposits. The carbonates of the Gádor and Felix units are highly permeable. The schist, phyllite and quartzite of both Alpujarride units are practically impermeable. With respect to the post-orogenic materials, the Miocene and Pliocene calcarenite and the Quaternary materials, are also permeable.

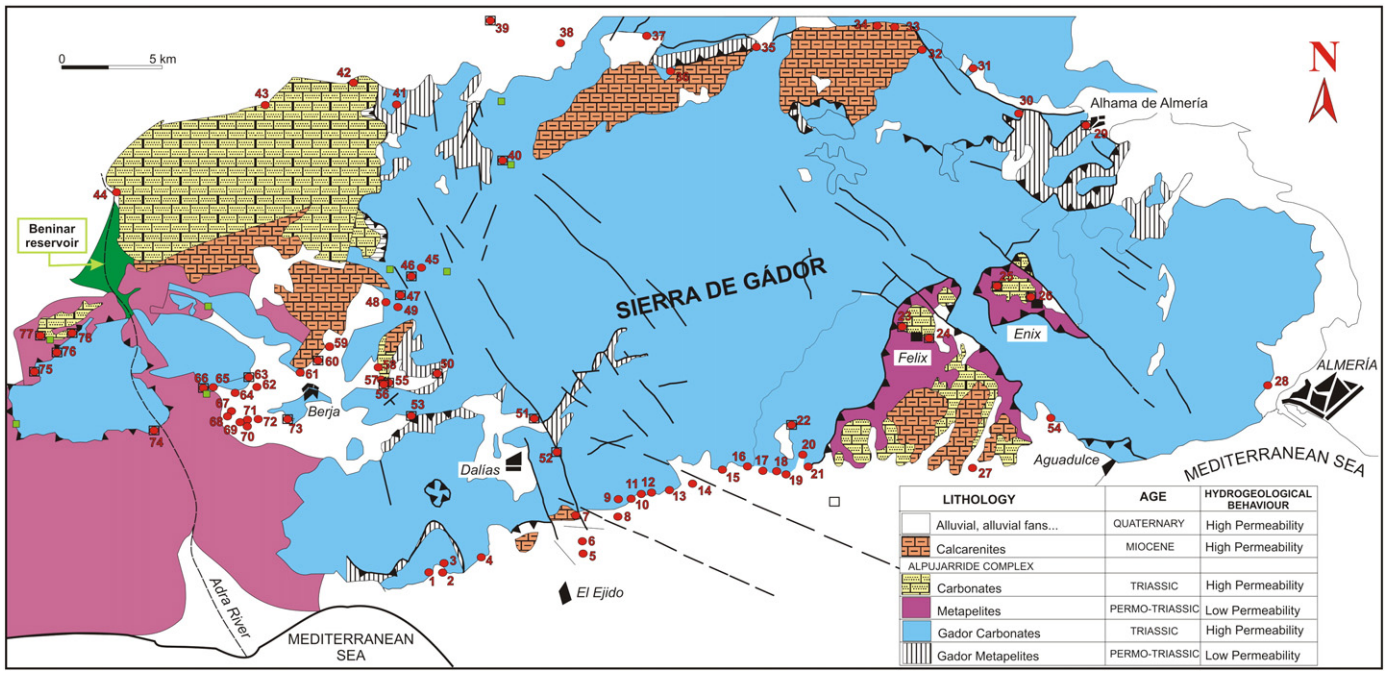

Fig. 1. Location of the study area and sampled points (red dots: hydrochemical analysis; red dots + square: tritium analysis; green square: D and ^{18}O from rainfall).

The Sierra de Gádor aquifers are geometrically complex as a consequence of the intense alpine compressional tectonics of the region.

Numerous reconnaissance boreholes have provided evidence of their structural complexity by revealing the variable thicknesses of quaternary materials and the faulting, which has resulted in substantial vertical and horizontal compartmentalization of the carbonate rocks.

The intense exploitation to which the Sierra de Gádor and Berja Basin have been subject is reflected in the aquifer units by falls in the piezometric level, deterioration in water quality and seawater intrusion (Molina et al., 2002, 2003).

3. Materials and methods

A sampling survey was carried out to monitor water quality and assess the main physicochemical processes in this aquifer. In July 2009, 78 samples of groundwater were collected from springs and wells (Fig. 1). Temperature, electrical conductivity (EC), and pH were determined in situ. Alkalinity (as HCO_3) was determined by titration at the time of sampling. Samples were taken in duplicate, filtered using a 0.45 μm Millipore filter and stored in polyethylene bottles at 4 °C. For cation analysis, one bottle of each sample was acidified to pH <2 with environmental grade (ultra-pure) nitric acid to avoid problems of absorption or precipitation. Sample composition was determined by means of an ICP-Mass Spectrometer at Acme Labs (Vancouver, Canada). The detection limits for Ca, Na, K, Mg, Cl, and S of the ICP-ES/ICP-MS method are: $1.24E10^{-3}$, $2.17E10^{-3}$, $1.27E10^{-3}$, $2.05E10^{-3}$, $2.82E10^{-2}$, and $1.04E10^{-2}$ mmol/L, respectively. The analytical results obtained are summarized in Table 1.

An extensive spatial network of sampling points was established to study the isotopic composition of the groundwater (for oxygen 18 and deuterium; Table 2). Samples were taken on two occasions (July 2008 and March 2010). Eight rain gauge stations were installed at different altitudes, ranging from 447 to 1455 m a.s.l., and rainwater samples were collected from July 2008 to February 2010 using homemade precipitation collectors. Each collector consisted of a funnel and a plastic container, adding paraffin oil (liquid petroleum) to avoid evaporation loss. After measuring the amount of meteoric water in the collector, the samples were stored in polyethylene bottles for later analysis at the Laboratory of Stable Isotopes in the Interdepartmental Research Service (SIDI), at the Universidad Autónoma de Madrid (Spain). Isotopic ratios were measured using an IRMS (Isotope Ratio Mass Spectrometer). Results, expressed as isotopic deviation δ (‰), were calculated according to the following equation:

$$\delta(‰) = \frac{(R_{sample} - R_{V\,SMOW})}{R_{V\,SMOW}} \times 10^3$$

where R_{sample} is the isotopic ratio ($^2H/^1H$, $^{18}O/^{16}O$) of the sample and $R_{V\,SMOW}$ is the isotope ratio of the international standard reference (Gonfiantini, 1981). The standard used was the Vienna Standard Mean Ocean Water (VSMOW; Gonfiantini, 1978). Analytical uncertainty was ±0.2 for $\delta^{18}O$, and ±0.5 for δ^2H.

The mean weighted ^{18}O and deuterium (^2H) composition of rainfall at each rain gauge was determined according to Paternoster et al. (2008):

$$R_{mw} = \frac{\sum_{i=1}^{n} P_i\,\delta X_i}{\sum_{i=1}^{n} P_i}$$

where P_i is the precipitation of the ith day, n is the number of days and δX_i refers to either δ^2H or $\delta^{18}O$ composition.

Twenty-three groundwater samples were collected for ^3H analysis in July 2007 in 1 L high-density polyethylene bottles. The samples were analysed at the University of Miami Tritium Laboratory (USA). Tritium was measured by internal Gas Proportional Counting of H^2-gas made from the water sample. Low-level water samples go through an electrolytic enrichment step whereby tritium concentrations are increased about 60-fold by means of volume reduction. Accuracy of the low-level measurement with enrichment is 0.10 TU (0.3 pCi L^{-1} of H_2O).

For the analysis of the carbon-13 composition of the dissolved inorganic carbon component (DIC), 72 water samples were taken in plastic bottles, which were fully filled to avoid carbon exchange between atmospheric carbon dioxide and bicarbonate in the water. ^{13}C isotope measurements were determined using a Finnigan Mat 251 at the Stable Isotope Laboratory of the Zaidin Experimental Station (Granada, Spain). The delta notation for ^{13}C is:

$$\delta^{13}C(‰) = \left(\frac{R_{sample}}{R_{V\,PDB}} - 1\right) \times 10^3$$

where R_{sample} and $R_{V\,PDB}$ are, respectively, the ratio of ^{13}C isotope abundance in the DIC of the water samples and in the Pee Dee Belemnite standard of Vienna, V PDB. The experimental error found was ±0.1‰.

The mineral saturation indices (SI) indicate the degree of saturation in a particular mineral phase compared to the aqueous solution in contact. Based on this SI value, the trend of precipitation or dilution of the mineral phases can be deduced. The SI was obtained using the PHREEQC code, version 3 (Parkhurst & Appelo, 2013). According to the characteristics of the study plot, the phases analysed were calcite, dolomite, gypsum, and halite.

4. Results and discussion

4.1. Hydrochemical characterization

The analytical results obtained are summarized in Table 1. Water in this aquifer displays a wide range in salinity, as indicated by the electrical conductivity (EC), which varies from 259 μS/cm to 3380 μS/cm. The samples with the highest salinity were taken close to the coastline, on the eastern and western limits of the study area. Groundwater temperature ranged between 8.9 °C and 42.5 °C. The highest thermal anomalies are probably due to deep flows related to intense fracturing (Morell et al., 2008). The pH ranged from 6.6 to 9.1, with the highest values corresponding to spring water.

Analytical data were plotted on a modified Durov diagram. In this version of the diagram, the cation and anion triangles are recognized and are separated along the 25% axes so that the main field is conveniently divided into nine subfields (Al-Bassam & Khalil, 2012; Al-Bassam et al., 1997). This diagram shows also the main chemical processes that can affect to water as ion exchange, dissolution or mixing water. Four groups are identified corresponding to four different hydrochemical types in the samples (Fig. 2). Group G-1 is characterized by calcium bicarbonate samples with low mineralization. G-2 contains samples that are more magnesic than in G1, apparently affected by a process of dolomite dissolution. The calcium–magnesium–bicarbonate facies from groups (G-1 and G-2) indicates recharge from limestone and dolostone. Group 3 shows the influence of sulphate dissolution and samples have a higher saline content than G-1 or G-2. G-4 contains the samples with the highest saline content, some of which have a sodium chloride facies (due to marine intrusion). Samples in this group indicate water that has undergone reverse ion exchange. The spatial distribution of the samples shows that both G-1 and G-2 occur throughout the Sierra; G-3 is centred on the western sector of the Sierra, with the majority of sampling points falling in the Berja basin. Samples from G-4 come from the southern edge of the Sierra, from areas relatively close to the coastline.

The groups identified from the Durov diagram are shown on the Piper diagram (Fig. 3). It would have been difficult to establish these groups based solely on a Piper diagram: group G-1 members lie parallel

Table 1
Results of chemical and isotopic analyses of water samples. Water samples for chemical analyses were taken in July 2009. EC: electrical conductivity. Location of sampling points in Fig. 1.

Sample	T (°C)	EC µS/cm	pH	Cl	SO_4	HCO_3	Na	Mg	Ca	K	$\delta^{13}C$ ‰	T	$\delta^{18}O$ ‰	δD‰	$\delta^{18}O$ ‰	δD‰	Group
				meq/L								TU	July 2008		March 2010		
1	26	1549	7,44	11,42	1,34	4,10	6,00	5,43	3,99	0,09	−9,33		−7,13	−47,11			G4
2	25,4	1115	7,55	6,77	1,28	4,20	3,62	4,29	3,38	0,08	−8,65		−7,58	−46,63			G4
3	25,3	782	7,88	2,00	1,58	4,80	1,78	3,25	3,18	0,07	−9,38		−8,10	−51,32			G2
4	24,1	827	7,53	3,47	1,23	4,70	2,15	3,64	3,16	0,08	−8,06		−8,13	−53,25			G2
5	27,4	1080	7,71	6,43	1,11	4,70	4,41	3,53	2,77	0,14	−7,59		−8,30	−54,63			G4
6	24,2	1040	7,85	5,16	0,86	4,10	2,32	4,07	3,78	0,05	−9,81		−8,13	−51,65			G4
7	22,8	557	7,7	0,87	0,89	4,60	0,77	2,69	2,71	0,03	−10,55		−8,24	−52,71			G2
8	24,2	670	7,54	2,71	0,81	4,20	1,48	3,13	2,56	0,07	−8,02		−8,21	−52,68			G2
9	21,8	403	7,66	0,76	0,42	3,40	0,56	2,08	1,94	0,02	−8,94		−7,88	−50,53			G2
10	21,6	460	7,72	1,21	0,40	3,60	0,91	2,18	2,08	0,03	−10,19		−7,81	−49,39			G2
11	21,5	419	7,63	0,76	0,44	3,60	0,59	2,18	2,07	0,03	−9,42		−8,13	−51,87			G2
12	20,9	459	7,6	0,90	0,38	3,90	0,67	2,34	2,30	0,02	−7,87		−8,19	−52,15			G2
13	20,5	453	7,56	0,79	0,52	4,00	0,60	2,41	2,24	0,02	−9,70		−8,14	−51,05			G2
14	26,1	502	7,44	0,59	0,73	4,60	0,53	2,89	2,52	0,05	−7,13		−8,41	−52,96			G2
15	22,8	548	7,62	0,93	0,70	4,90	0,71	2,47	2,72	0,14	−10,18		−8,34	−52,85			G2
16	22,7	570	7,46	0,73	1,06	4,90	0,60	3,17	2,90	0,05	−5,97		−8,26	−53,65			G2
17	23,3	664	7,64	1,69	0,84	4,60	1,20	2,93	2,66	0,17	−10,03		−8,22	−52,12			G2
18	21,5	1046	7,91	6,46	0,84	4,20	3,09	3,38	4,00	0,03	−9,38		−8,97	−56,88			G4
19	20,7	1579	7,58	9,28	1,20	4,20	6,09	3,93	5,27	0,15	−8,56		−8,93	−56,59			G4
20	22,5	1072	7,35	5,95	1,05	5,00	2,89	3,85	4,32	0,03	−10,29		−8,52	−54,61			G3
21	15,9	3380	7,49	22,09	2,06	3,50	17,24	6,49	7,42	0,08			−8,91	−57,58			G4
22	16,8	541	7,42	0,73	0,18	5,70	0,45	2,29	3,50	0,02	−9,39	2,43	−7,49	−48,05			G1
23	17,3	326	8,17	0,31	0,12	3,20	0,30	2,10	1,57	0,01		5,17					G3
24	18,9	449	7,7	0,62	0,75	4,10	0,52	2,11	2,42	0,13	−11,58	4,31	−7,28	−46,39			G2
25	16,3	390	7,76	0,34	0,16	4,30	0,29	2,43	2,01	0,01	−10,60	2,51	−7,68	−49,49			G2
26	17,4	394	7,8	0,48	0,41	4,40	0,36	2,51	1,80	0,01	−11,40	5,77	−7,29	−45,99			G2
27	22,6	2930	7,55	21,44	6,09	5,20	16,15	7,86	5,72	0,18	−7,49		−6,29	−44,03			G4
28	27,8	1266	7,55	7,22	1,87	5,20	6,64	3,76	2,25	0,24	−8,68		−6,62	−44,74			G4
29	42,5	915	7,03	0,54	4,53	6,30	0,84	3,51	6,18	0,11	−2,50		−8,41	−55,07			G1
30	30,9	932	7,36	0,42	4,68	7,30	0,39	3,93	6,37	0,24	−5,88		−8,46	−54,98			G1
31	28,9	839	7,19	0,42	2,93	7,30	0,47	4,06	5,27	0,18	−4,80		−8,42	−55,11			G1
32	22,7	939	6,98	0,71	1,93	10,10	0,41	5,79	6,24	0,12	−3,03		−8,31	−55,52			G2
33	22,7	980	7,08	0,45	2,51	9,20	0,36	5,12	6,48	0,03	−3,65		−8,36	−52,40			G1
34	24,1	967	7,01	0,34	3,79	8,40	0,32	4,92	6,13	0,08	−3,38		−8,49	−55,64			G1
35	18,2	561	7,55	0,28	0,73	6,20	0,21	2,88	3,16	0,09	−10,42		−8,44	−55,97			G2
36	20,1	599	7,68	0,28	1,13	6,00	0,30	3,24	3,53	0,03	−9,74		−8,09	−52,75			G2
37	16,7	538	8,44	0,25	1,66	4,65	0,27	2,47	3,87	0,02	−11,19		−8,91	−57,31			G1
38	19,1	765	7,85	0,48	3,56	5,70	0,67	2,96	5,75	0,03			−8,77	−54,78			G1
39	15,2	368	7,58	0,17	1,28	3,10	0,16	1,35	2,74	0,06	−9,22		−9,02	−56,95			G1
40	12,1	259	8,18	0,11	0,07	3,60	0,06	1,47	1,54	0,01	−11,26	5,05	−9,39	−60,11			G1
41	14,4	271	7,97	0,20	0,28	2,65	0,14	1,47	1,54	0,01	−12,02		−8,81	−56,31			G2
42	23,2	859	7,16	0,48	3,75	6,80	0,78	4,31	5,66	0,07	−8,36		−8,59	−54,75			G1
43	20,6	676	7,95	0,68	2,35	5,00	1,01	3,18	3,76	0,04	−9,66		−8,35	−52,68			G2
44	24,1	740	8,71	1,27	3,18	4,05	1,79	3,13	3,64	0,08	−9,36		−7,95	−53,82	−9,86	−70,24	G3
45	8,9	301	8,07	0,08	0,37	3,10	0,06	1,23	1,93	0,06	−8,32				−7,54	−51,91	G1
46	17,1	345	8,42	0,14	1,36	2,70	0,16	1,63	1,90	0,01	−10,78	2,56			−8,04	−57,34	G1
47	17,8	356	8,12	0,25	0,88	3,40	0,32	1,93	2,10	0,01	−10,20	1,93			−8,70	−60,15	G2
48	23,4	844	7,41	1,21	2,55	6,10	1,27	4,41	3,62	0,10	−6,04		−8,09	−55,58			G2
49	23,7	384	8,43	0,23	0,69	3,30	0,32	1,86	2,07	0,01	−10,90				−8,74	−60,58	G2
50	16,7	483	8,09	0,20	2,26	3,30	0,12	2,23	2,92	0,09	−5,30	0,90			−9,42	−65,29	G1
51	16,7	302	7,93	0,14	0,22	3,50	0,09	1,65	1,80	0,01	−10,33	0,92	−9,51	−59,49	−9,35	−63,68	G1
52	15,2	300	8,13	0,14	0,27	3,80	0,08	1,68	1,77	0,01	−9,28	0,55	−9,57	−60,87	−9,40	−64,35	G2
53	20,6	536	7,75	0,39	1,72	4,00	0,50	2,49	2,76	0,03	−10,99	0,67	−8,59	−53,59	−8,25	−57,24	G2
54	24,1	1735	7,4	9,79	1,51	4,70	6,21	4,94	5,71	0,06	−8,69						G4
55	18,5	553	7,71	0,17	2,75	3,40	0,18	2,14	3,06	0,06	−7,52	0,69	−9,59	−63,14	−9,35	−64,47	G1
56	18	557	7,87	0,23	2,94	3,40	0,15	2,47	3,58	0,12	−9,16	0,77	−9,63	−61,90	−9,53	−64,88	G1
57	17,1	542	7,85	0,28	2,83	3,30	0,16	2,74	3,54	0,02	−7,96				−9,42	−65,31	G1
58	17,9	611	7,69	0,42	2,62	3,90	0,62	2,80	3,36	0,02	−6,12				−8,31	−58,32	G2
59	21,1	1072	7,47	1,47	2,65	6,50	1,76	6,15	3,81	0,08	−9,17						G2
60	20,3	761	7,47	0,45	3,50	5,90	0,50	3,53	4,55	0,13	−4,46	0,68			−8,98	−62,10	G4
61	20,3	734	7,52	0,39	3,60	4,60	0,41	3,40	4,43	0,14	−9,08				−9,24	−63,22	G1
62	20,3	1479	7,26	1,18	9,52	1,90	1,00	10,30	6,97	0,41	−10,01				−8,55	−59,42	G3
63	24,2	1428	7,46	3,55	6,69	5,60	2,71	6,96	6,18	0,09	−8,75	0,63			−8,40	−59,40	G3
64	22,4	1464	7,48	4,32	3,81	4,78	0,96	5,10	4,34	1,41	−7,65						G3
65	22,7	1228	7,34	3,07	4,54	5,30	2,94	5,52	4,83	0,11	−6,90				−7,73	−54,81	G3
66	21,9	1155	7,45	2,99	4,46	4,40	2,82	4,65	4,93	0,13	−7,40	0,47			−8,32	−58,50	G3
67	20,1	1556	7,27	1,83	10,73	6,10	1,41	9,55	8,09	0,18	−9,30						G3
68	21,5	1478	7,3	1,33	7,59	6,60	1,45	8,85	7,92	0,10	−11,31						G3
69	19,2	2260	7,18	3,41	13,84	7,60	2,10	15,72	10,82	0,20	−10,39				−7,48	−53,73	G3
70	20,4	1782	7,17	1,92	10,22	7,60	1,89	11,15	9,17	0,17	−10,69						G3
71	19,7	1853	7,23	1,97	9,68	7,80	1,97	11,91	9,16	0,14	−9,57						G3
72	20,2	1701	7,1	2,12	10,61	7,30	1,71	10,60	9,15	0,09					−7,82	−56,28	G3
73	20,3	974	7,5	0,85	4,45	5,25	1,17	5,08	5,28	0,15	−8,77	1,00			−8,50	−59,70	G3

(continued on next page)

Table 1 (*continued*)

Sample	T (°C)	EC µS/cm	pH	Cl	SO_4	HCO_3	Na	Mg	Ca	K	$\delta^{13}C$ ‰	T	$\delta^{18}O$ ‰	δD‰	$\delta^{18}O$ ‰	δD‰	
				meq/L								TU	July 2008		March 2010		Group
74	24,4	2530	8,01	10,41	11,78	5,60	10,00	6,66	12,64	0,21	−7,59	2,47	−8,47	−56,89	−9,19	−64,15	G3
75	16,5	415	6,62	0,45	0,44	3,90	0,47	2,21	1,56	0,11	−7,65	5,07			−7,58	−49,20	G2
76	18,3	329	8,05	0,31	0,27	3,30	0,19	1,60	1,55	0,11	−12,10	4,66			−7,21	−47,13	G2
77	17,9	343	8,3	0,37	0,45	3,20	0,26	2,16	1,07	0,13	−8,02	4,42			−7,21	−47,38	G2
78	20,3	331	9,12	0,45	0,33	3,30	0,28	1,68	1,39	0,18	−11,80	4,41			−7,01	−46,52	G2

to one edge of the diagram as a result of their sulphate content, although some samples are concentrated in the vertex corresponding to the bicarbonate ion. That is to say, not all samples in group G-1 are affected by sulphate dissolution. Group G-2 demonstrates a more magnesic cation content. Group G-3 is characterized by a spread of anion composition, although the sulphate concentration is generally higher in these samples. As commented above, group G-4 is characterized by it mostly sodium-chloride facies.

Ionic ratios were examined in an attempt to establish the hydrogeochemical processes that influence the physico-chemical composition of the samples. Fig. 4a shows the Ca + Mg–SO_4 versus bicarbonate ratios. The goal of this relationship is to observe the carbonate dissolution processes (limestone and dolostone). Removing the groundwater SO_4 concentration, the sulphate dissolution interference can be avoided. Samples with the lowest concentrations are aligned with a 1:1 ratio, indicating dolomite dissolution, but at concentrations greater than 5 meq/L HCO_3 the samples (G-3 and G-4) deviate from the theoretical line. Other processes also affect the position of these samples on the graph. Fig. 4b shows that group G-3 lies close to the 1:1 straight line on a graph of HCO_3 + SO_4 against Ca + Mg. The carbonate and sulphate

Table 2
Results of $\delta^{18}O$, δD, and D-excess of each rainfall station. P: Precipitation in mm.

Sample	Date		P (mm)	$\delta^{18}O_{VSMOW}$	δD_{VSMOW}	Altitude (m)	D-excess
	From	To					
MP1	08-Jul-08	02-Oct-08	76,4	−6,48	−45,2		
	02-Oct-08	25-Feb-09	127,3	−9,40	−63,8		
	25-Feb-09	23-Apr-09	87,9	−8,78	−61,3		
	23-Apr-09	29-Jul-09	22,3	−3,38	−30,2		
	29-Jul-09	23-Oct-09	111,4	−8,74	−60,3		
	23-Oct-09	10-Feb-10	127,3	−9,32	−67,6		
	Mean weighted			−8,50	−59,6	1383	8,38
MP2	08-Jul-08	02-Oct-08	70,0	−5,17	−34,3	920	7,28
	17-Dec-08	25-Feb-09	127,3	−9,31	−61,7		
	25-Feb-09	23-Apr-09	57,3	−7,66	−56,6		
	23-Apr-09	29-Jul-09	19,1	−1,97	−21,0		
	29-Jul-09	23-Oct-09	63,7	−7,53	−54,6		
	23-Oct-09	10-Feb-10	127,3	−8,38	−61,3		
	Mean weighted			−7,68	−54,2		
MP3	04-Dec-08	18-Feb-09	127,3	−7,35	−50,2	447	3,06
	18-Feb-09	16-Apr-09	40,7	−6,98	−51,0		
	16-Apr-09	28-Jul-09	12,1	−1,20	−23,6		
	28-Jul-09	24-Oct-09	57,3	−6,97	−55,4		
	24-Oct-09	06-Feb-10	127,3	−6,41	−51,5		
	Mean weighted			−6,72	−50,7		
MP4	04-Dec-08	18-Feb-09	127,3	−8,03	−53,1	702	5,25
	18-Feb-09	16-Apr-09	58,6	−7,54	−56,1		
	16-Apr-09	28-Jul-09	20,4	−2,97	−29,8		
	28-Jul-09	24-Oct-09	72,6	−7,01	−55,7		
	24-Oct-09	03-Feb-10	127,3	−7,81	−58,1		
	Mean weighted			−7,45	−54,4		
MP5	04-Dec-08	18-Feb-09	127,3	−9,50	−63,9	1208	9,21
	18-Feb-09	22-Apr-09	52,2	−9,17	−64,9		
	22-Apr-09	28-Jul-09	7,0	−3,96	−37,7		
	28-Jul-09	24-Oct-09	66,2	−8,74	−63,1		
	24-Oct-09	06-Feb-10	127,3	−7,84	−54,0		
	Mean weighted			−8,66	−60,1		
MP6	12-Dec-08	18-Feb-09	127,3	−8,38	−55,9	527	5,78
	18-Feb-09	22-Apr-09	41,4	−7,28	−53,9		
	22-Apr-09	31-Jul-09	10,2	−0,62	−19,7		
	31-Jul-09	23-Oct-09	47,7	−7,16	−56,0		
	23-Oct-09	10-Feb-10	127,3	−7,83	−58,4		
	Mean weighted			−7,67	−55,5		
MP7	12-Dec-08	25-Feb-09	127,3	−8,96	−60,1	1005	8,26
	25-Feb-09	29-Apr-09	56,0	−7,61	−55,7		
	29-Jul-09	23-Oct-09	7,6	−8,10	−61,5		
	23-Oct-09	10-Feb-10	127,3	−8,22	−59,1		
	Mean weighted			−8,21	−57,4		
MP8	12-Dec-08	25-Feb-09	127,3	−9,94	−66,0	1455	10,40
	25-Feb-09	04-May-09	58,6	−8,72	−60,4		
	29-Jul-09	23-Oct-09	76,4	−9,47	−67,0		
	23-Oct-09	10-Feb-10	127,3	−8,65	−60,4		
	Mean weighted			−9,24	−63,5		

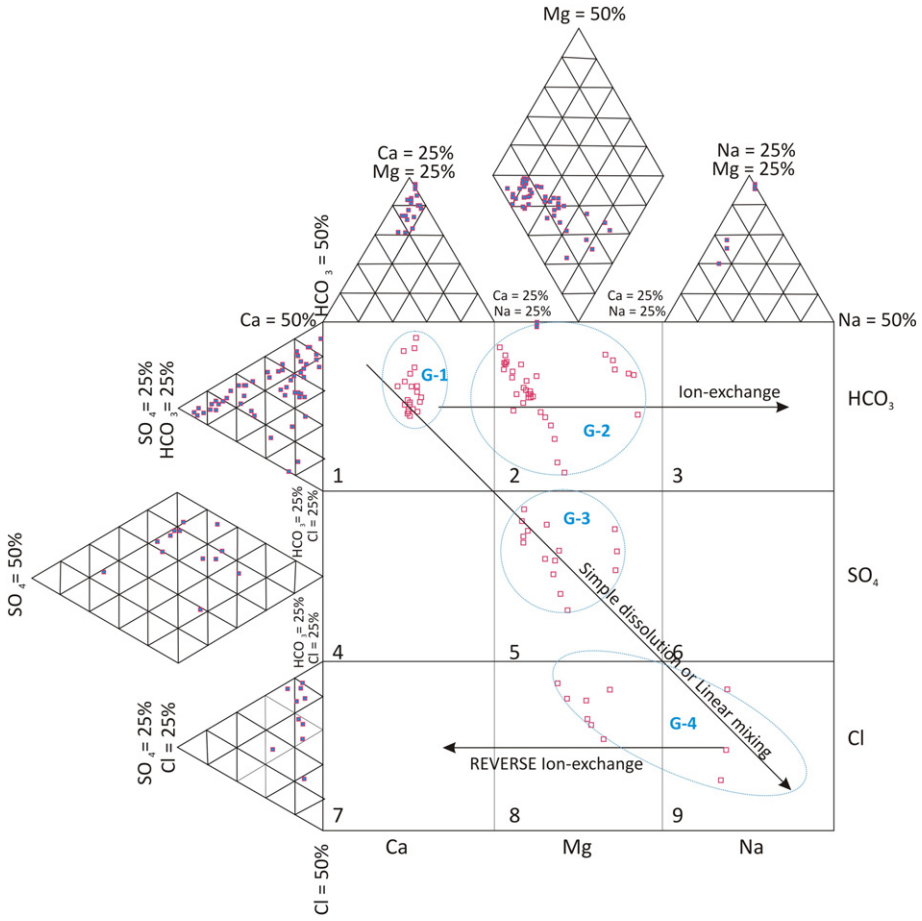

Fig. 2. Expanded Durov diagram corresponding to groundwater samples.

dissolution processes can be detected using this plot. Samples of group G-4, characterized by their basically sodium chloride composition, are distributed all along the Ca + Mg axis. This excess in Ca + Mg is consisted to the deficit in Na observed in Fig. 4c. The plot of Cl vs. Na related to marine influence on the processes under study (Fig. 4c), shows how the most saline samples in group G-4 lie below the line of 1:1 mixing, indicating a deficit in Na related to the reverse ion exchange ($CaX + 2Na^{+} \rightarrow 2NaX + Ca^{2+}$).

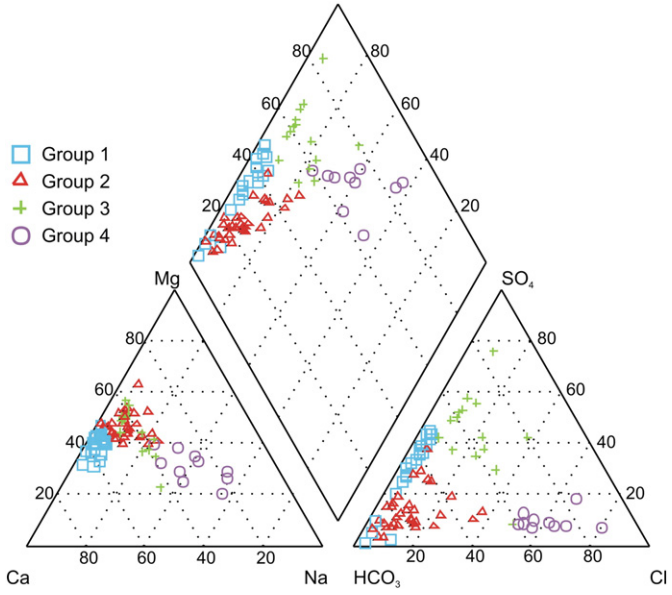

Fig. 3. Piper diagram. Samples have been grouped according to the groups identified in Durov diagram.

The saturation indices (SI) give a quantitative description of the deviation of the water away from equilibrium with respect to dissolved minerals. The changes in saturation state can be used to distinguish different stages of hydrochemical evolution, as well as to identify the geochemical reactions that determine water chemistry. Approximately 95% of the SI values for calcite and dolomite in the groundwater samples were greater than zero. The samples that are both saturated with respect to calcite and dolomite imply a greater dissolution and stronger mineralisation. Fig. 5a shows this relationship, SI calcite vs. SI dolomite. It indicates a linearity. This linear relationship excludes extensive gypsum dissolution process which should have altered the saturation levels of both minerals. Slight oversaturation of many of the waters with respect to calcite is expected under conditions of dedolomitization, necessary to cause precipitation of calcite (Plummer et al., 1990). The SIs are lower in calcite than in dolomite, probably because calcium is being precipitated, while the solution continues being saturated in dolomite. The dominant process affecting all samples, regardless of group (G-1 to G-4), is carbonate dissolution. The saturation of gypsum evolves simultaneously with SO_4 contents (Fig. 5b). However, the SI values of gypsum and anhydrite are less than zero, indicating that these minerals remain subsaturated. Similar results have been found in the karstic basin, southwest China (Wu et al., 2009), where gypsum does not reach its saturation point, and thus the dedolomization in the aquifer continues in the study area. Group G-3 gives the highest values, due to the dissolution of sulphate salts. The samples from G-4 have a higher salinity being less subsaturated in halite than the others (Fig. 5c).

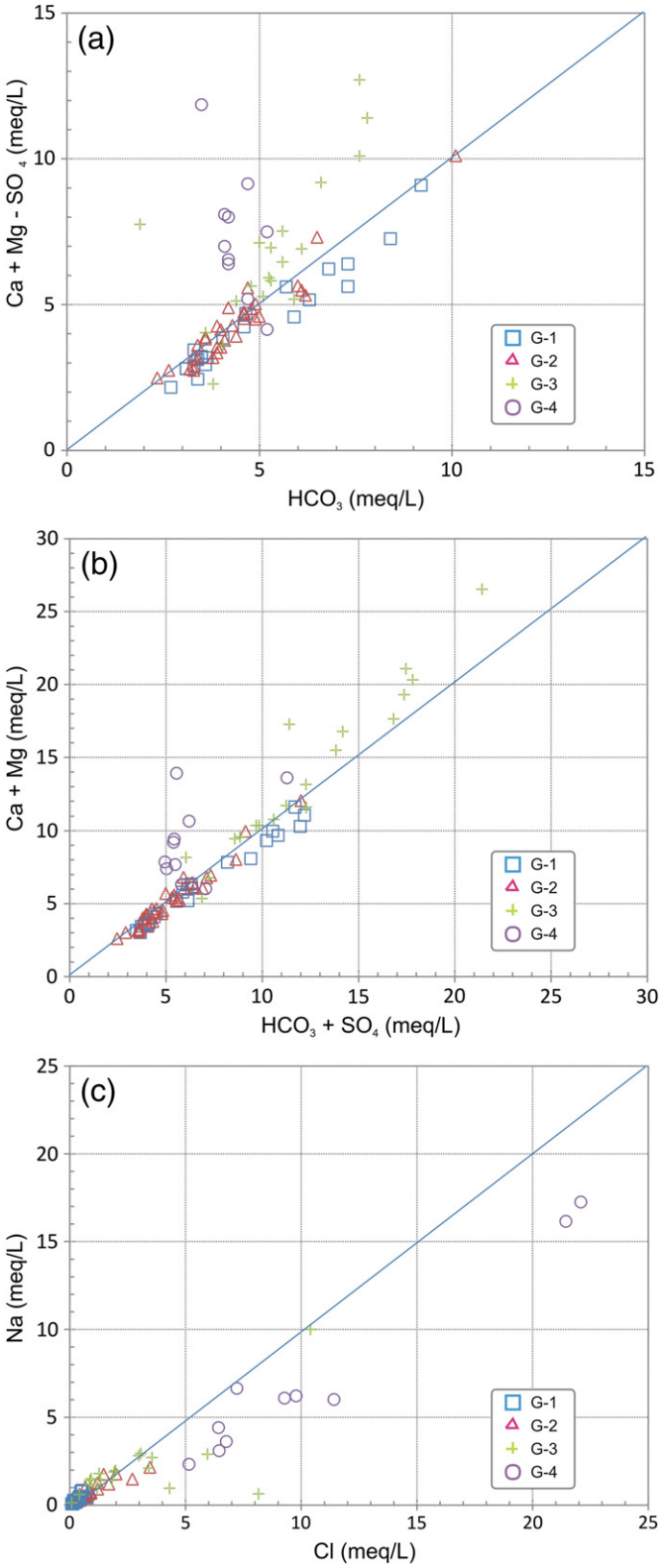

Fig. 4. Hydrochemical relationships between selected ions in groundwater. Dissolution line has been included.

Apparently, in group G-3, the influence of carbonate dissolution is not as strong, being masked by the presence of sulphates in the medium. The 1:1 ratio for SO_4–Ca suggests dissolution of $CaSO_4$ (gypsum).

$$CaSO_4 \rightarrow Ca^{2+} + SO_4^{2-} \quad (1)$$

Group G-3 fits fairly well to this straight line (Fig. 6a). The existence of interbedded gypsum could explain the presence of sulphate waters. This is not to say that the main process acting on the rock is not carbonate dissolution. The excess of calcium is clearly obvious in groups G-1, G-2, and G-4 but less so in samples from G-3. Carbonate dissolution is important for producing G-1, G-2, and G-4 samples, while for G3 waters gypsum dissolution plays an important role. Fig. 6b, which shows the relationship between Mg and HCO_3, allows us to clarify which processes determine the ion distribution of the samples. A ratio of 1:4 indicates congruent dissolution of dolomite, while a ratio below 0.25 would suggest a simultaneous dissolution of calcite and dolomite. It is generally agreed that dissolution of magnesium carbonates takes place significantly within the saturated zone, under closed-system conditions (Appelo & Postma, 2005; Clark & Fritz, 1997).

Groups G-1 and G-2 are slightly about the ratio 1:4. Nevertheless, samples in group G-3 clearly have an excess of magnesium. The process that could explain this is dedolomitization. An excess of dissolved calcium is produced as a consequence of the dissolution of gypsum; it provokes the precipitation of calcite, so increasing the quantity of dissolved magnesium (Back et al., 1983; Deike, 1990; Ma et al., 2011; Saunders & Toran, 1994). The net result is that the dissolution of gypsum induces the transformation of dolomite to calcite in the rock and produces waters with increased Mg^{2+}, Ca^{2+}, and SO_4^{2-} concentrations. In the case of group G-4, the samples are evenly distributed above the 1:4 line, possibly due to the presence of magnesium from a marine origin. Fig. 6c shows the ratio of Cl to Mg and indicates linearity between these two for the samples in group G-4.

To decipher the processes affecting groups G-1 and G-2, slightly affected by sulphate dissolution, Fig. 6d displays the ratio of the non-gypsum sourced Ca^{2+} (Ca^{2+}–SO_4^{2-}) vs. HCO_3^-. Samples in groups G-1 and G-2 lie close to the 1:4 straight line, corresponding to dolomite dissolution, while higher values in this relationship would be a consequence of calcite and dolomite dissolution. However, most of these samples are below this line. This Ca deficiency can be balanced with the Mg excess detected in these samples (Fig. 6b). The dedolomitization is likely affecting to these samples, though not forgetting that the main process that affects groups G-1 and G-2 is dolomite dissolution.

4.2. Isotope geochemistry

During recent years, a number of isotope studies have been carried out to characterize the hydrogeology of local aquifers in south-eastern Spain (Andreo et al., 2004; Cerón et al., 2000; Cruz-San Julian et al., 1992; Frot et al., 2007; Vallejos et al., 1997; Vandenschrick et al., 2002). The LMWL (Local Meteoric Water Line) obtained in the study area is $\delta D = 5.2891\delta^{18}O - 15.157$ with $R^2 = 0.967$. Fig. 7a and Table 2 illustrate the δ values, which range from −0.62‰ to −9.94‰ for ^{18}O and −19.7‰ to −67.6‰ for deuterium (D). The isotopic values for precipitation are spread over a wide range, due mainly to the high seasonal variability that is a well-known climatic feature of the Mediterranean area (Grassa et al., 2006; Liotta et al., 2006; 2013). That way, there are some variations in deuterium excess from precipitation. It may be a consequence of evaporation during precipitation and continental moisture recycling, regional processes that control these variations (Froehlich et al., 2008). The local meteoric water line, based on the mean weighted ^{18}O and deuterium (D) composition of rainfall (WLMWL, Weighted Local Meteoric Water Line), is $\delta D = 5.0798\delta^{18}O - 16.21$ with $R^2 = 0.984$ (Fig. 7b).

In contrast, groundwater shows a narrower range of isotopic signals ($\delta^{18}O$ from −6.29‰ to −9.86‰; δD from −44.03‰ to −70.24‰). This is explained by the hydrological characteristics of the aquifers, which tend to favour the mixing of meteoric waters with different recharge times. This feature is also reflected in a narrower seasonal variability of groundwater. In Fig. 8, which shows the ratio $^{18}O/D$, we can see how the groundwaters are distributed between the global meteoric

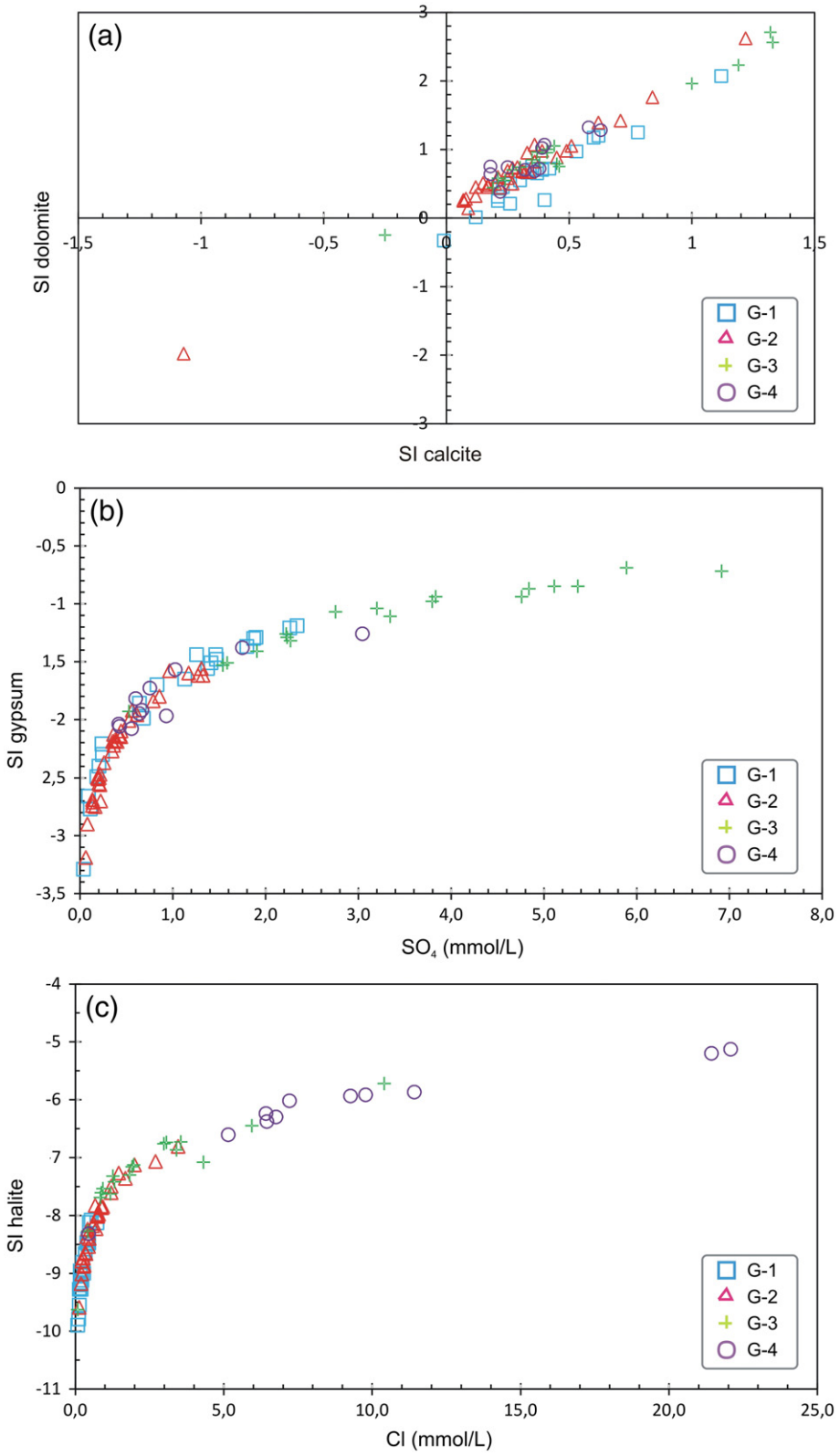

Fig. 5. (a) Saturation index (SI) of groundwater with respect to calcite and dolomite. (b) SI gypsum vs SO_4. (c) SI halite vs Cl.

line ($\delta D = 8\delta^{18}O + 10$, GMWL; Craig, 1961) and the Mediterranean meteoric line ($\delta D = 8\delta^{18}O + 13.7$, MMWL) established by Celle-Jeanton et al. (2001). Based on this graph, three sectors can be distinguished according to the isotope signal recorded. These are for ^{18}O from −8.98‰ to −9.86‰ in Sector 1, from −7.63‰ to −8.97‰ in Sector 2 and from −6.29‰ to −7.88‰ in Sector 3.

The mean isotopic gradient with altitude can be determined directly from the rainwater samples collected at a series of sites located at different altitudes (Table 2). The altitude effect has been used to estimate the mean elevation of recharge over the whole of Sierra de Gádor. The magnitude of this effect on the isotopic composition of the precipitation depends on the climate and local topography. The isotope gradients, as a

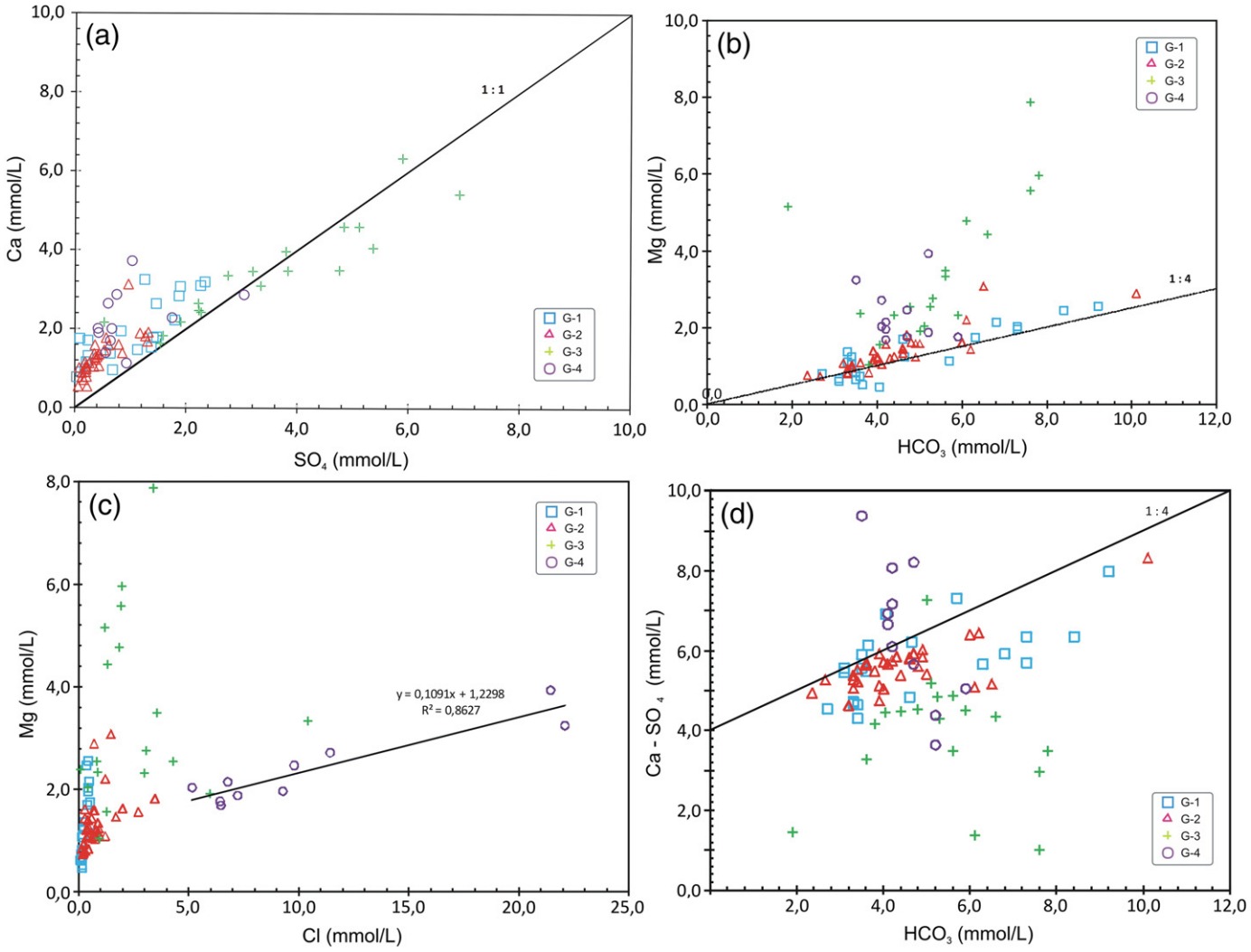

Fig. 6. Hydrochemical relationships between selected ions in groundwater. Dissolution line has been included.

function of altitude, change seasonally and the correction has been considered for the distribution of the altitude within the recharge area (Holdsworth et al., 1991). The value of the $\delta^{18}O$-altitude gradient is −0.19‰/100 m. This relationship is shown in Fig. 9. According to the sectors identified from the $\delta^{18}O$–δD graph (Fig. 8), the recharge altitudes corresponding to each sector are: 2000–1500 m a.s.l., 1500–900 m a.s.l., and below 900 m a.s.l. Sector 1 corresponds to the highest recharge band (2000–1500 m a.s.l.), represented by samples taken from springs in the west of the Sierra, which is where the highest mountains are. Samples from less than 900 m a.s.l. (Sector 3) correspond to springs that drain small tectonic klippen and boreholes located in the eastern part of the Sierra. The remaining samples are from points distributed on both the northern and southern faces of the Sierra de Gádor, where recharge occurs at altitudes of between 900 and 1500 m a.s.l. (Sector 2).

Environmental isotopes ($\delta^{13}C$ and ^{3}H) together with hydrochemical parameters were used to understand the hydrochemical evolution and, hence, the residence times of groundwater contained within the aquifer of Sierra de Gádor. The groundwater shows the greatest variation in $\delta^{13}C_{DIC}$ signatures, which vary from −2.5‰ to −12.1‰ (Table 1), with an average of −8.7‰ $\delta^{13}C_{DIC}$. In terms of tritium, many of the samples do not register any tritium, which indicates a long transit time between the moment recharge occurred and the moment the water is taken from a boreholes or discharged from a spring. A number of aquifer points were chosen where it was considered tritium could be detected and the results are given in Table 1. The ratio $\delta^{13}C/^{3}H$ allows samples to be classified according to the reaction time (or residence time) in the aquifer (Fig. 10). The pluviometric recharge has mixed completely with the pre-existing water and stored water. This mixing frequently reduces the tritium concentration and masks the presence of modern recharge water. Samples with tritium concentrations of less than 1 TU indicate a longer transit time in the aquifer, while higher tritium values and values indicating impoverishment relative to ^{13}C, indicate shorter residence times. In general, these samples coincide with water recharged at lower altitude and discharged via springs. In the easternmost sector, high tritium values were detected and this indicates the zone with the greatest influence of modern recharge, i.e., there is a preferential circulation of groundwater corresponding to present-day marine intrusion (Vallejos et al., 1997). As in Gran Sasso, Central Italy, the isotopes provide additional information about groundwater flowpaths and hydrodynamics in fissured and karstic aquifers (Barbieri et al., 2005).

The relationship between groundwater flow, the main hydrogeochemical processes, recharge altitude and transit time is summarized in Fig. 11.

5. Conclusions

The hydrogeochemistry of the water samples from the Sierra de Gádor aquifer system indicates four different types, each was

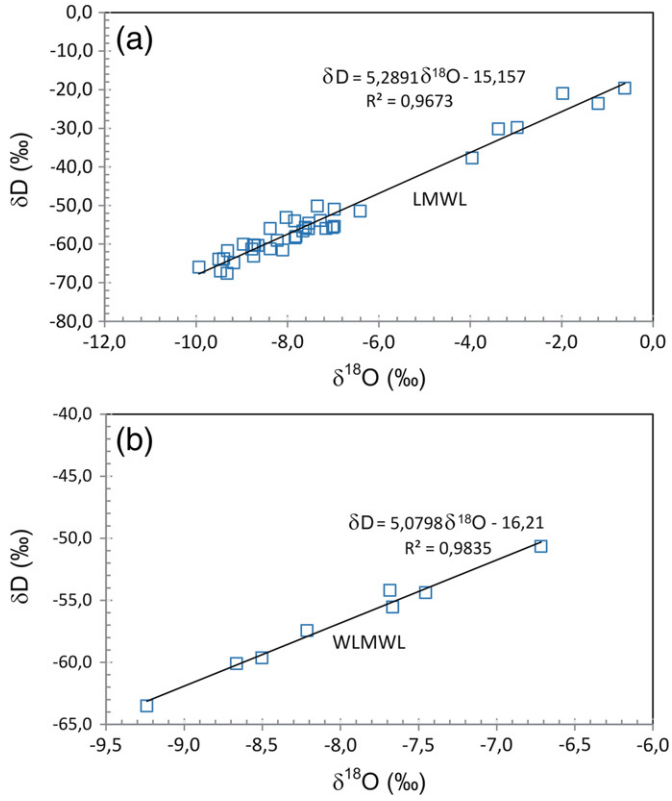

Fig. 7. (a) Plot of D versus ^{18}O contents of the precipitation samples collected in Sierra de Gádor from July 2008 to October 2009 (LMWL: Local Meteoric Water Line). (b) Plot based on the mean weighted ^{18}O and deuterium (D) composition of the precipitation samples (WLMWL: Weighted Local Meteoric Water Line).

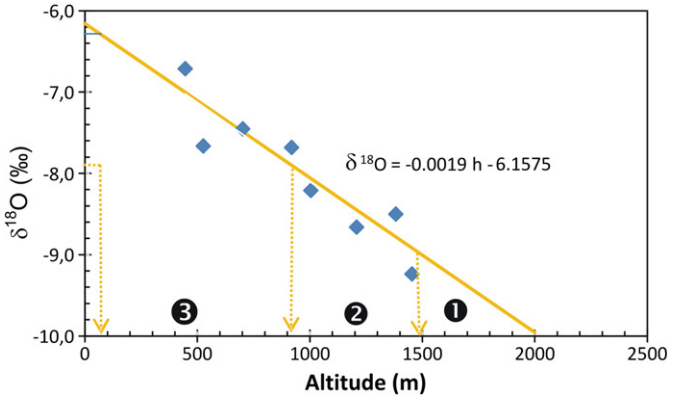

Fig. 9. $\delta^{18}O$ plotted versus altitude in order to obtain the overall vertical gradient and the principal recharge areas, based on the isotopic composition of groundwater.

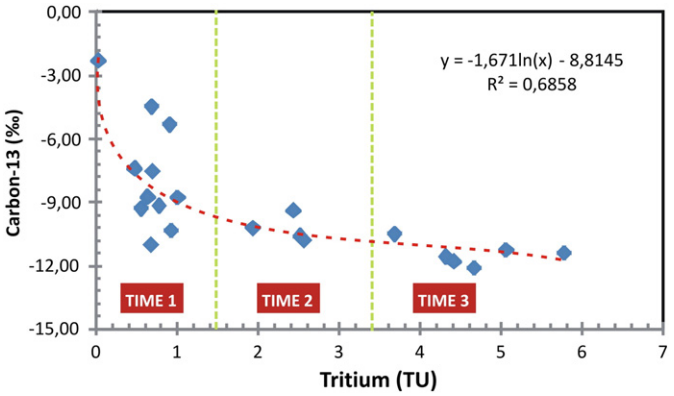

Fig. 10. Variation of $\delta^{13}C$ (in HCO_3) with the tritium concentration of groundwater. Time 1 to Time 3 indicates from the longest to shortest transit time in the aquifer.

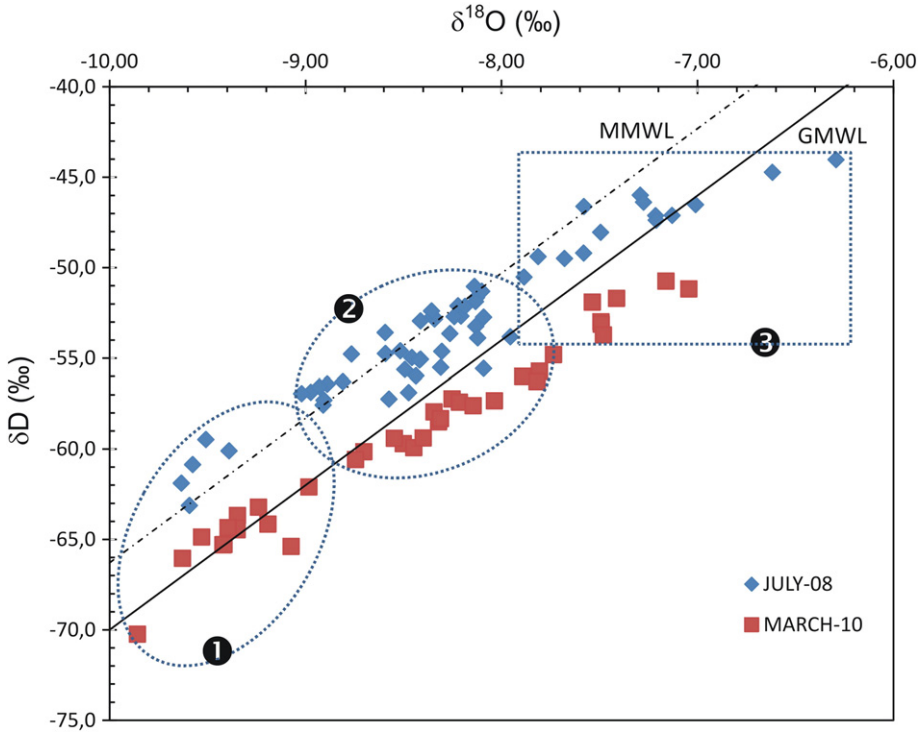

Fig. 8. $\delta D/\delta^{18}O$ relationship of groundwater samples collected in Sierra de Gádor in July 2008 and March 2010 (GMWL: Global Meteoric Water Line, MMWL: Mediterranean Meteoric Water Line).

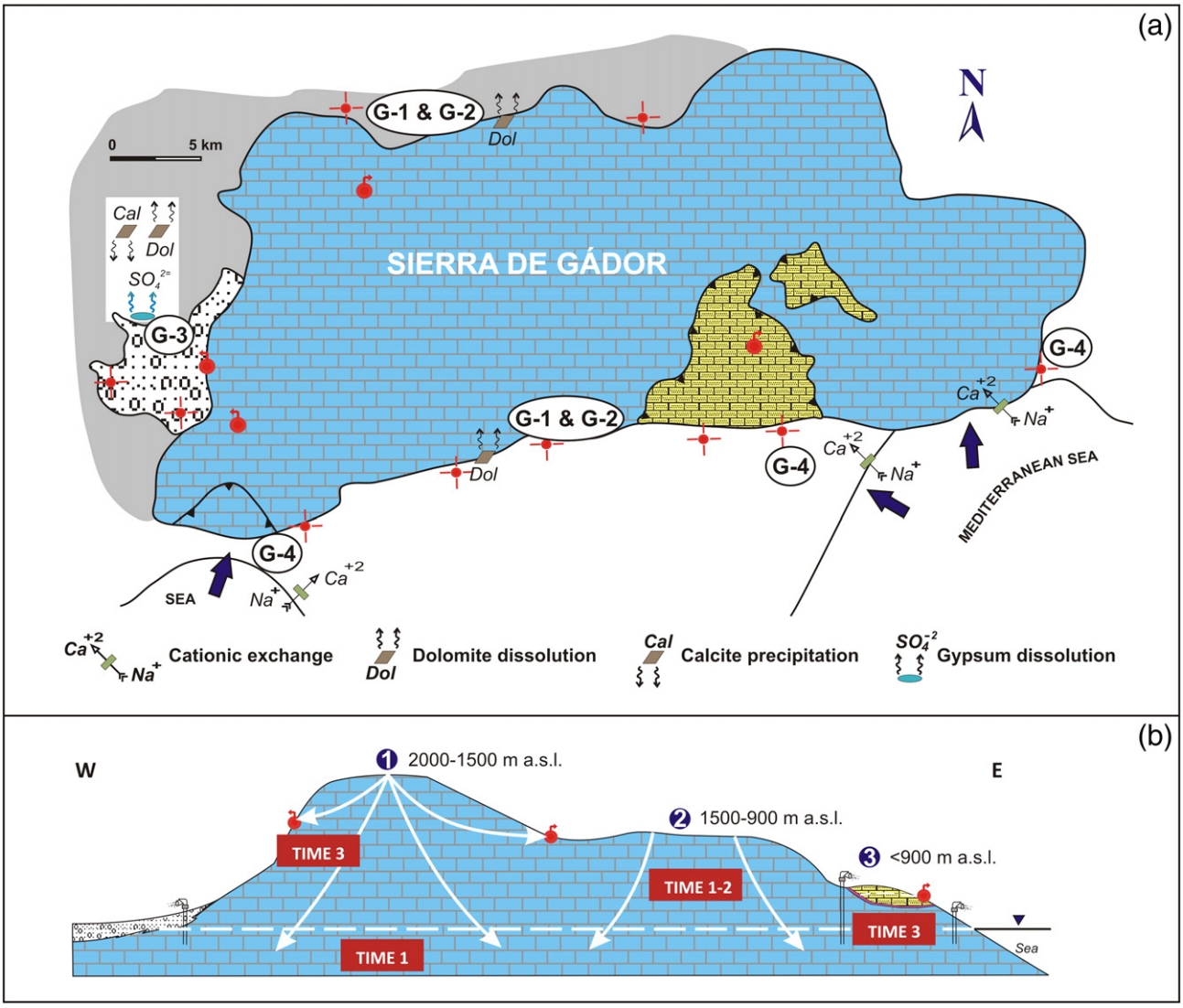

Fig. 11. Scheme of hydrogeochemical processes (a) and recharge area and transit time (b) in Sierra de Gádor aquifer system. The numbers 1 to 3 in Fig. 11b correspond to the main recharge areas.

characterized by a series of hydrogeochemical processes and a particular location within the macrosystem (Fig. 11a). The reactions that occur, due to the lack of equilibrium between the aqueous and solid phases in the aquifer, correspond to processes of carbonate precipitation–dissolution, ion exchange as a consequence of seawater intrusion, and input of sulphates. Group G-1 corresponds to low-mineralization waters and calcium bicarbonate facies; group G-2 has a similar composition to G-1 but is more magnesic, its waters having been affected by a process of dolomite dissolution. Both G-1 and G-2 groups are the result of dissolution of carbonates; sampling points in these groups come from both the northern and southern faces of the Sierra. Group G-3 is characterized by greater salinity, linked to sulphate dissolution (gypsum) and an excess of magnesium. These characteristics can be explained by a process of dedolomitization. That is to say, as a consequence of gypsum dissolution, an excess of dissolved calcium is produced, which provokes the precipitation of calcite and increases the quantity of dissolved magnesium. Samples placed in this group come from the western part of the Sierra. Lastly, group G-4 is an agglomerate of the most saline samples, which mostly have a sodium chloride facies due to the fact that these samples are affected by marine intrusion, in which the principal process in operation is reverse ion exchange. This exchange requires the presence of a rock with exchangeable calcium and water higher in sodium; effect generally observed with seawater intrusion. It results in the release of calcium (and sometimes magnesium) and a decrease in sodium. Sampling points falling in this group come from either the eastern or western coastal boundaries of the aquifer, with their physicochemical composition being explained by the presence of marine intrusion at these points.

By means of the isotope composition of both precipitation and groundwater samples, we have detected three main recharge areas in the carbonate aquifer (Fig. 11b). The residence time of water in the aquifer is several years, though in some cases more recent recharge is detected, arising from rainwater infiltration or seawater intrusion. In the sector corresponding to the highest recharge altitude (2000–1500 m a.s.l.), two flow systems were identified – one deep and the other shallower. The more superficial one, evinced from tritium concentrations, discharges via springs. The sector corresponding to recharge at altitudes lower than 900 m a.s.l. corresponds to springs that drain small klippen, and to borehole samples from the eastern sector of the Sierra, whose tritium content may be explained by seawater intrusion. The intermediate sector between these two corresponds to recharge altitudes of 1500–900 m a.s.l., where the flow may be deep or shallow and the residence time short or long. The methodology applied in this study, using major ion chemistry and isotope composition, provides an integrated understanding of this groundwater carbonate system.

References

Al-Bassam, A.M., Khalil, A.R., 2012. DurovPwin: a new version to plot the expanded Durov diagram for hydro-chemical data analysis. Comput. Geosci. 42, 1–6.

Al-Bassam, A.M., Awad, H.S., Al-Alawi, J.A., 1997. DurovPlot a computer program for processing and plotting hydro-chemical data. Groundwater 35 (2), 362–367.

Andreo, B., Liñán, C., Carrasco, F., Jiménez de Cisneros, C., Caballero, E., Mudry, J., 2004. Influence of rainfall quantity on the isotopic composition (^{18}O and ^{2}H) of water in mountainous areas. Application for groundwater research in the Yunquera-Nieves karst aquifers (S Spain). Appl. Geochem. 19, 561–574.

Appelo, C.A.J., Postma, D., 2005. Geochemistry, Groundwater and Pollution. 2nd ed. A.A. Balkema, Leiden, The Netherlands (649 pp.).

Back, W., Hanshaw, B.B., Plummer, L.N., Rahn, P.H., Rightmire, C.T., Rubin, M., 1983. Process and rate of dedolomitization: mass transfer and ^{14}C dating in a regional carbonate aquifer. Geol. Soc. Am. Bull. 94, 1415–1429.

Barbieri, M., Boschetti, T., Petitta, M., Tallini, M., 2005. Stable isotopes (^{2}H, ^{18}O and $^{87}Sr/^{86}Sr$) and hydrochemistry monitoring for groundwater hydrodynamics analysis in a karst aquifer (Gran Sasso, Central Italy). Appl. Geochem. 20, 2063–2081.

Capaccioni, B., Didero, M., Paletta, C., Salvadori, P., 2001. Hydrogeochemistry of groundwaters from carbonate formations with basal gypsiferous layers: an example from the Mt Catria–Mt Nerone ridge (Northern Appennines, Italy). J. Hydrol. 253, 14–26.

Cardenal, J., Benavente, J., Cruz-San Julián, J.J., 1994. Chemical evolution of groundwater in Triassic gypsum bearing carbonate aquifers (Las Alpujarras, South Spain). J. Hydrol. 161, 3–30.

Celle-Jeanton, H., Travi, Y., Blavoux, B., 2001. Isotopic typology of the precipitation in the Western Mediterranean region at three different time scales. Geophys. Res. Lett. 28 (7), 1215–1218.

Cerón, J.C., Martín-Vallejo, M., García-Rossell, L., 2000. CO2-rich thermomineral groundwater in the Betic Cordilleras, southeastern Spain: genesis and tectonic implications. Hydrogeol. J. 8 (2), 209–217.

Clark, I., Fritz, P., 1997. Environmental Isotopes in Hydrogeology. Lewis Publishers, New York (328 pp.).

Craig, H., 1961. Isotopic variations in meteoric waters. Science 133, 1702–1703.

Cruz-San Julian, J., Araguás, L., Rozanski, K., Benavente, J., Cardenal, J., Hidalgo, M.C., García-López, S., Martínez-Garrido, J.C., Moral, F., Olías, M., 1992. Sources of precipitation over southeastern Spain and groundwater recharge. an isotopic study. Tellus 44B, 226–236.

Daniele, L., Vallejos, A., Corbella, M., Molina, L., Pulido-Bosch, A., 2013. Geochemical simulations to assess water–rock interactions in complex carbonate aquifers: the case of Aguadulce (SE Spain). Appl. Geochem. 29, 43–54.

Deike, R.G., 1990. Dolomite dissolution rates and possible Holocene dedolomitization of water-bearing units in the Edwards aquifer, South-Central Texas. J. Hydrol. 112, 335–373.

Froehlich, K., Kralik, M., Papesch, W., Rank, D., Scheifinger, H., Stichler, W., 2008. Deuterium excess in precipitation of Alpine regions — moisture recycling. Isot. Environ. Health Stud. 44 (1), 1–10.

Frot, E., van Wesemael, B., Vandenschrick, G., Souchez, R., Sole-Benet, A., 2007. Origin and type of rainfall for recharge of a karstic aquifer in the western Mediterranean: a case study from the Sierra de Gador-Campo de Dalias (southeast Spain). Hydrol. Process. 21, 359–368.

Gat, J.R., 1996. Oxygen and hydrogen stable isotopes in the hydrological cycle. Annu. Rev. Earth Planet. Sci. 24, 225–262.

Gat, J.R., Airey, P.L., 2006. Stable water isotopes in the atmosphere/biosphere/lithosphere interface: scaling-up from the local to continental scale, under humid and dry conditions. Global Planet. Chang. 51, 25–33.

Gonfiantini, R., 1981. The δ-notation and the mass-spectrometric measurement techniques. In: Gat, J.R., Gonfiantini, R. (Eds.), Stable Isotope Hydrology. Deuterium and Oxygen-18 in the Water Cycle. Technical Reports Series No. 210, pp. 35–84.

Gonfiantini, R., 1978. Standards for stable isotope measurements in natural compounds. Nature 271, 534–536.

Grassa, F., Favara, R., Valenza, M., 2006. Moisture source in the Hyblean Mountains region (south-eastern Sicily, Italy): evidence from stable isotopes signature. Appl. Geochem. 21, 2082–2095.

Hanshaw, B.B., Back, W., 1979. Major geochemical processes in the evolution of carbonate-aquifer systems. J. Hydrol. 43, 287–312.

Herczeg, A.L., Leaney, F.W.J., Stadler, M.F., Allan, G.L., Fifield, L.K., 1997. Chemical and isotopic indicators of point-source recharge to a karst aquifer, South Australia. J. Hydrol. 192, 271–299.

Holdsworth, G., Fogarasi, S., Krouse, H.R., 1991. Variation of the stable isotopes of water with altitude in the Saint Elias Mountains of Canada. J. Geophys. Res. 96 (D4), 7483–7494.

Hunkeler, D., Mudry, J., 2007. Hydrochemical methods. In: Goldscheider, N., Drew, D. (Eds.), Methods in Karst Hydrogeology. IAH 26, pp. 93–121.

Kanduč, T., Mori, N., Kocman, D., Stibilj, V., Grassa, F., 2012. Hydrogeochemistry of Alpine springs from North Slovenia: insights from stable isotopes. Chem. Geol. 300–301, 40–54.

Kendall, C., McDonnell, J.J., 1998. Isotope Tracers in Catchment Hydrology. Elsevier, Amsterdam.

Kohfahl, C., Sprenger, C., Benavente, J.B.H., Meyer, H., Fernández Chacón, F., Pekdeger, A., 2008. Recharge sources and hydrogeochemical evolution of groundwater in semiarid and karstic environments: a field study in the Granada Basin (Southern Spain). Appl. Geochem. 23, 846–862.

Ladouche, B., Luc, A., Dörfliger, N., 2009. Chemical and isotopic investigation of rainwater in Southern France (1996–2002): Potential use as input signal for karst functioning investigation. J. Hydrol. 367, 150–164.

Lee, E.S., Krothe, N.C., 2001. A four-component mixing model for water in karst terrain in south-central Indiana, USA, using solute concentration and stable isotopes as tracers. Chem. Geol. 179, 129–143.

Liotta, M., Favara, R., Valenza, M., 2006. Isotopic composition of the precipitations in the central Mediterranean: origin marks and orographic precipitation effects. J. Geophys. Res. 111, D19302.

Liotta, M., Grassa, F., D'Alessandro, W., Favara, R., Gagliano Candela, E., Pisciotta, A., Scaletta, C., 2013. Isotopic composition of precipitation and groundwater in Sicily, Italy. Appl. Geochem. 34, 199–206.

López-Chicano, M., Bouamama, M., Vallejos, A., Pulido-Bosch, A., 2001. Factors which determine the hydrogeochemical behaviour of karstic springs. a case study from the Betic Cordilleras, Spain. Appl. Geochem. 16, 1179–1192.

Ma, R., Wang, Y., Sun, Z., Zheng, C., Ma, T., Prommer, H., 2011. Geochemical evolution of groundwater in carbonate aquifers in Taiyuan, Northern China. Appl. Geochem. 26 (5), 884–897.

Martin-Rojas, I., Somma, R., Delgado, F., Estevez, A., Iannace, A., Perrone, V., Zamparelli, V., 2009. Triassic continental rifting of Pangaea: direct evidence from the Alpujarride carbonates, Betic Cordillera, SE Spain. J. Geol. Soc. 166, 447–458.

Martín-Rosales, W., Gisbert, J., Pulido-Bosch, A., Vallejos, A., Fernández-Cortés, A., 2007. Estimating groundwater recharge induced by engineering systems in a semiarid area (southeastern Spain). Environ. Geol. 52, 985–995.

Mazor, E., 1991. Applied Chemical and Isotopic Groundwater Hydrology. Halsted Press, New York (274 pp.).

Molina, L., Vallejos, A., Pulido-Bosch, A., Sánchez-Martos, F., 2002. Water temperature and conductivity variability as indicators of groundwater behaviour in complex aquifer systems in the south-east of Spain. Hydrol. Process. 16, 3365–3378.

Molina, L., Sánchez-Martos, F., Pulido-Bosch, A., Vallejos, A., 2003. Origin of boron from a complex aquifer in Southeast of Spain. Environ. Geol. 44, 301–307.

Moral, F., Cruz-Sanjulián, J.J., Olias, M., 2008. Geochemical evolution of groundwater in the carbonate aquifers of Sierra de Segura (Betic Cordillera, southern Spain). J. Hydrol. 360, 281–296.

Morell, I., Pulido-Bosch, A., Sánchez-Martos, F., Vallejos, A., Daniele, L., Molina, L., Calaforra, J.M., Roig, A.F., Renau, A., 2008. Characterization of the salinisation processes in aquifers using boron isotopes; application to south-eastern Spain. Water Air Soil Pollut. 187 (1–4), 65–80.

Nhan, D.D., Van Lam, N., Long, H.C., Thuan, D.D., Minh, D.A., Anh, V.T., 2013. Hydrological characteristics of karstic groundwater in the northeast Vietnam as studied by isotopic techniques. Environ. Earth Sci. 70, 521–529.

Parkhurst, D.L., Appelo, C.A.J., 2013. Description of input and examples for PHREEQC version 3—a computer program for speciation, batch-reaction, one-dimensional transport, and inverse geochemical calculations. U.S. Geological Survey Techniques and Methods, Book 6 (chap. A43, 497 pp., available only at http://pubs.usgs.gov/tm/06/a43/).

Paternoster, M., Liotta, M., Favara, R., 2008. Stable isotope ratios in meteoric recharge and groundwater at Mt. Vulture volcano, southern Italy. J. Hydrol. 348, 87–97.

Plummer, L.N., Busby, J.F., Lee, R.W., Hanshaw, B.B., 1990. Geochemical modeling of the Madison aquifer in parts of Montana, Wyoming and South Dakota. Water Resour. Res. 26 (9), 1981–2014.

Prtoljan, B., Kapelj, S., Dukarić, F., Vlahović, I., Mrinjek, E., 2012. Hydrogeochemical and isotopic evidences for definition of tectonically controlled catchment areas of the Konavle area springs (SE Dalmatia, Croatia). J. Geochem. Explor. 112, 285–296.

Pu, T., He, Y., Zhang, T., Wu, J., Zhu, G., Chang, L., 2013. Isotopic and geochemical evolution of ground and river waters in a karst dominated geological setting: a case study from Lijiang basin, South-Asia monsoon region. Appl. Geochem. 33, 199–212.

Rodríguez-Fernández, J., Martín-Penela, A.J., 1993. Neogene evolution of the Campo de Dalias and surrounding off-shore areas (Northeastern Alboran Sea). Geodin. Acta 6, 255–270.

Sanz de Galdeano, C., Rodriguez-Fernández, J., López-Garrido, A.C., 1985. A strike-slip fault Corridor within the Alpujarra Mountains (Betic Cordilleras, Spain). Geol. Rundsch. 74, 641–655.

Saunders, J.A., Toran, L.E., 1994. Evidence for dedolomitization and mixing in Paleozoic carbonates near Oak Ridge, Tennessee. Ground Water 32 (2), 207–214.

Vallejos, A., Pulido Bosch, A., Martín Rosales, W., Calvache, M.L., 1997. Contribution of environmental isotopes to the understanding of complex hydrologic systems. a case study: Sierra de Gádor, SE Spain. Earth Surf. Process. Landf. 22, 1157–1168.

Vandenschrick, G., van Wesemael, B., Frot, E., Pulido-Bosch, A., Molina, L., Stievenard, M., Souchez, R., 2002. Using stable isotope analysis (δD–$\delta^{18}O$) to characterise the regional hydrology of the Sierra de Gador, S-E Spain. J. Hydrol. 265, 43–55.

Wicks, C.M., Herman, J.S., 1996. Regional hydrogeochemistry of a modern coastal mixing zone. Water Resour. Res. 32 (2), 401–407.

Wu, P., Tang, C., Zhu, L., Lui, C., Cha, X., Tao, X., 2009. Hydrogeochemical characteristics of surface water and groundwater in the karst basin, southwest China. Hydrol. Process. 23, 2012–2022.